A Numerical Simulation of Barotropic Instability. Part I: Wave–Mean Flow Interaction[1]

MARK R. SCHOEBERL

Laboratory for Planetary Atmospheres, NASA/Goddard Space Flight Center, Greenbelt, MD 20771

RICHARD S. LINDZEN

Department of Earth, Atmospheric and Planetary Sciences, Massachusetts Institute of Technology, Cambridge, MA 02139

(Manuscript received 6 September 1983, in final form 11 January 1984)

ABSTRACT

A numerical model is used to study the evolution of the barotropic point jet instability as it interacts with the mean flow. The linearized instability solution agrees well with the recent analytical solutions of Lindzen.

Stabilization of the point jet instability occurs as the mean flow is modified by wave vorticity transport. Assuming stabilization occurs when the meridional gradient of the zonal mean vorticity is no longer negative, the maximum integrated wave enstrophy can be predicted. In addition, an estimate of the integrated wave enstrophy at steady state can be made by balancing the generation of vorticity against dissipation. These limits are found to be in good agreement with the numerical results.

1. Introduction

Barotropic and baroclinic instabilities are the processes through which momentum and heat are redistributed within a symmetric vortex by Rossby waves. The barotropic instability, which propagates horizontally, chiefly transports momentum, while the (pure) baroclinic instability propagates vertically and transports heat. The study of these instabilities has been one of the principle objectives of dynamic meteorology over the last three decades as the baroclinic instability is the principle source for midlatitude synoptic-scale disturbances.

Although the pure baroclinic and barotropic instabilities have different physical interpretations, they are mathematically similar as has been demonstrated by Lindzen and Tung (1978) (hereafter LT) and Lindzen *et al.* (1983). The criteria for these instabilities cannot be derived from local (parcel) arguments like the Rayleigh-Taylor or inertial instability. As a result, the conditions describing Rossby wave stability are usually formulated from fluid integral theorems except for very special cases (Tung, 1981). The Rayleigh-Kuo and Fjortøft theorems are examples of such conditions (e.g., Charney and Stern, 1962).

For Rossby wave instability, the Rayleigh-Kuo theorem gives a necessary but not sufficient condition for instability requiring that $\partial\bar{q}/\partial y$ change sign somewhere within the fluid domain. Here $\bar{q}$ is the zonal mean pseudo-potential vorticity (pv), an approximation to Ertel's potential vorticity which is conserved on isobaric surfaces rather than potential isotherms; y is the northward coordinate.

At small amplitudes, unstable Rossby waves produce a flux of potential vorticity which appears to be redistributing $\bar{q}$ such that $\partial\bar{q}/\partial y$ would obtain the same sign everywhere. If this tendency continued as the wave reached finite amplitudes, the system would no longer be unstable so the wave would stop growing. We refer to this process as saturation or equilibration of the instability.

In linear instability studies, the change in $\bar{q}$ by wave fluxes is not allowed. However, we hypothesize that if wave–mean flow interaction is allowed, the system will proceed toward stabilization as suggested by the linear results. The final state may be unsteady and have finite amplitude waves present. (Indeed, they must be present for the problems posed below.) But, these latter situations are determined by the details of the posed problem. Some properties and constraints on the equilibration process is the subject of this paper.

Recently, LT and Lindzen *et al.* (1980) have interpreted the mechanics of Rossby wave instability as a manifestation of wave overreflection. The overreflection occurs when the wave, encountering a critical line (CL), is reflected with more energy than incident. If the same wave is repeatedly reflected from the CL, amplification of the disturbance occurs. The evidence for overreflection is simply that the wave energy flux is directed away from the CL. If the wave energy flux is directed toward the CL then the CL is a partial reflector or absorber. Analytic treatment of Rossby wave absorbing CL's in a stable ($\partial\bar{q}/\partial y > 0$) environment has been discussed by Dickinson (1968).

Although overreflection is intimately associated with the CL, it also depends on the propagation properties

[1] Contribution No. 9 of the Stratospheric General Circulation with Chemistry Modeling Project at NASA/GSFC.

of the adjacent fluid regions. This nonlocal character of overreflection is discussed in both LT and Lindzen *et al.* (1980). The conditions for overreflection summarized in LT are:

1) $\partial\bar{q}/\partial y$ changes sign somewhere in the domain (the Rayleigh-Kuo criteria).

2) A CL must exist within the domain. The CL does not have to be in a region of negative $\partial\bar{q}/\partial y$ and is usually located outside that region. This requirement follows from the arguments of Taylor (1915) and Bretherton (1966).

3) The overreflected wave must be contained to the extent that leakage along other boundaries does not result in more energy loss than that gained by overreflection.

Extensive application of overreflection theory to determine the dispersion curves for unstable Rossby waves has been used by Lindzen *et al.* (1980). These authors have primarily dealt with the classic Charney problem for baroclinic instability (Charney, 1947, 1973).

Lindzen *et al.* (1983) have shown that the point jet barotropic instability problem is the simplest flow which is homomorphic to the Charney problem. The quasi-nonlinear barotropic problem has been chosen for this study rather than the corresponding baroclinic problem because it is one-dimensional, involving only nonlinear modification of $\bar{u}(y)$, while the baroclinic problem is intrinsically two-dimensional, involving changes in $\bar{u}(y, z)$ and the static stability $N^2(z)$.

Even though the linear instability problem has been exhaustively investigated, the nonlinear problem, namely, the process through which the unstable Rossby wave may stabilize itself through nonlinear interaction, is less thoroughly understood. Numerical investigations of the nonlinear wave–mean flow behavior have been made by Simons (1972), Simmons and Hoskins (1978), Edmon *et al.* (1980) and others with regard to the life cycle of a baroclinic wave. The study by Edmon *et al.* (1980) also showed the utility of Eliassen and Palm (EP) flux diagnostics in differentiating the barotropic or baroclinic aspects of the Rossby wave instability. (In the real atmosphere and in general circulation models, most instabilities exhibit properties of both the pure baroclinic and barotropic instabilities.) The generalized wave–mean flow theorems developed by Andrews and McIntyre (1976, 1978) are especially useful in studying nonlinear aspects of instabilities. However, except in the generalized Lagrangian-mean framework, these theorems are mostly useful when the wave amplitude is small (i.e., when wave–wave interaction can be neglected).

Lindzen and Schoeberl (1982) and Schoeberl (1981) showed that the integrated enstrophy can be a useful diagnostic even for finite amplitude disturbances. This diagnostic will be applied to barotropic instability and its evolution as it interacts with the mean flow. For simplicity, in the models described below, wave–wave interaction is suppressed in the zonal spectrum; therefore, our results will differ from analyses where such interaction is included. Without wave–wave interaction, the zonal cascade of energy and enstrophy cannot occur and wave energy and enstrophy transfer take place only between the single unstable zonal harmonic and the mean flow. We have performed calculations with wave–wave interaction which suggest that wave–wave effects are not important for the present problem. The results of the wave–wave interaction studies will be reported in Part 2.

In Section 2, we shall examine the linearized point jet instability. Linearized means that wave–mean flow interaction is not allowed. In Section 3, we include wave–mean flow interaction in order to examine the evolution of the instability. Finally, in Section 4 we briefly discuss the role of dissipation on the wave–mean flow interaction and examine the situation where several waves interact with the mean flow but not with each other.

2. The linear instability

a. *Some general properties*

For a quasi-geostrophic system, potential vorticity q is conserved on isobaric surfaces. Thus,

$$\frac{d}{dt}(q)_p = S,$$

where

$$\frac{d}{dt} = \frac{\partial}{\partial t} + u\frac{\partial}{\partial x} + v\frac{\partial}{\partial y}$$

and S is a source or sink. The variables u and v are velocities in the x (eastward) and y (northward) directions. The potential vorticity for a barotropic system of constant depth on a β-plane is given by

$$q = f + \nabla^2\psi,$$

where $f = f_0 + \beta y$, is the Coriolis parameter. For a barotropic system, the potential vorticity is simply the vorticity, $\nabla^2 = \partial^2/\partial y^2 + \partial^2/\partial x^2$, and

$$u = -\partial\psi/\partial y, \quad v = \partial\psi/\partial x.$$

The wave–mean flow system (without wave–wave interaction) is

$$\frac{\partial}{\partial t}q' + \bar{u}\frac{\partial}{\partial x}q' + v'\frac{\partial\bar{q}}{\partial y} = S', \tag{1}$$

$$\frac{\partial}{\partial t}\bar{q} = -\frac{\partial}{\partial y}(\overline{v'q'}) + \bar{S}, \tag{2}$$

where $(\ )' = (\bar{\ }) - (\ )$ and $(\bar{\ })$ is a zonally (x) averaged quantity. For this study, $S' = -Dq'$ and $\bar{S} = -D(\bar{q} - q_0)$, where D is a generalized dissipation process in the form of Rayleigh friction; q_0 is the initial state.

Several useful relations can be derived from (1) and (2). If rigid boundaries exist at $y = 0$ and L, then multiplying (1) by q' and taking the zonal average gives

$$\frac{1}{2}\frac{\partial}{\partial t}(\overline{q'^2}) = -(\overline{v'q'})\frac{\partial \bar{q}}{\partial y} - D(\overline{q'^2}). \tag{3}$$

Furthermore, it is easily shown that

$$(\overline{v'q'}) = -\partial(\overline{u'v'})/\partial y. \tag{4}$$

Utilizing the boundary conditions

$$\int_0^L (\overline{v'q'})dy = 0 \tag{5a}$$

and Eq. (2) yields

$$\frac{\partial}{\partial t}\int_0^L \bar{q}dy = -\int_0^L D(\bar{q} - q_0)dy. \tag{5b}$$

If $D = 0$, the integrated pv is conserved exactly. The quantity $-(\overline{u'v'})$ is the horizontal component of the EP flux F while

$$A = \frac{(\overline{q'^2})}{2}\left(\frac{\partial \bar{q}}{\partial y}\right)^{-1} \tag{6}$$

is the wave action or EP wave activity (Andrews and McIntyre, 1978; Palmer, 1982). If the mean state is constant in time when (3) has the conservative form

$$\frac{\partial A}{\partial t} = -\frac{\partial}{\partial y}F,$$

so

$$\frac{\partial}{\partial t}\int_0^L A = 0.$$

From (4), using the form of the wave action equation, the wave action propagation velocity C_g may be defined as

$$C_g = F/A = -2\frac{(\overline{u'v'})}{(\overline{q'^2})}\frac{\partial \bar{q}}{\partial y}. \tag{7}$$

For linear waves in a slowly varying medium C_g corresponds to the group velocity.

The energy flux is given by $E_f = (\overline{v'\phi'})$, where $\phi' = f_0\psi' + \phi'_a$, and ϕ'_a is the ageostrophic component of the pressure. Using the zonal momentum equation, in the limit $c_i \to 0$, to determine the ageostrophic pressure we obtain

$$E_f = (\overline{v'\phi'}) = -(\bar{u} - c)(\overline{u'v'}), \tag{8}$$

where c is the phase speed of the wave in the zonal direction and c_i is the imaginary part of c. From the definition of F, i.e.,

$$F = E_f(\bar{u} - c)^{-1}. \tag{9}$$

Clearly, if $(\bar{u} - c) > 0$ then F and E_f have the same sign, but in the region $(\bar{u} - c) < 0$, F and E_f have opposite signs. For Rossby waves where c_i, $D = 0$ then F and E_f will always have the same sign since wave propagation is not allowed in the region $(\bar{u} - c) < 0$ (Charney and Drazin, 1961.) However, for gravity waves, propagation can occur for both signs of $(\bar{u} - c)$. Thus, the EP flux may be oppositely directed to the energy flux for some types of gravity waves (e.g., the Kelvin inertio–gravity wave).

In the case of unstable Rossby waves, $(\bar{u} - c)$ may be less than zero over a substantial part of the fluid. For example, in the baroclinic problem this region is the zone below the steering level (where $\bar{u} = c$). In that zone, the EP flux is upward and wave action is advected vertically [see Fig. 1 in Edmon *et al.* (1980)], but the energy flux is downward. Therefore, C_g as defined by (7) can be linked with wave action flux only in the Rossby wave instability problem and does not give the direction of the energy flux.[2]

b. *The point jet*

The zonal wind function for the point jet is defined by

$$\bar{u} = \Gamma|y - y_0| + u_0, \tag{10}$$

where $y_0 = L/2$. In the numerical calculations to follow, $u_0 = -25$ m s^{-1}, $\Gamma = 10^{-5}$ s^{-1}, $L = 5000$ km and an equatorial value for β is used. The profile of the point jet is shown in Fig. 1a. Using (10), we have

$$\frac{\partial \bar{q}}{\partial y} = \beta - 2\Gamma\delta(y - y_0), \tag{11}$$

where $\delta(y)$ is the Dirac delta function. Letting

$$\psi' = \psi'(y)e^{im(x-ct)}$$

where the double use of ψ' should not present difficulties, Eq. (1) becomes

$$\frac{\partial^2\psi'}{\partial y^2} + \frac{\psi'}{(\bar{u} - c)}\frac{\partial \bar{q}}{\partial y} - m^2\psi' = 0. \tag{12}$$

Integrating (12) across the δ function and taking ψ' continuous at y_0 we obtain the interface condition

$$\left.\frac{\partial\psi'}{\partial y}\right|_{y_0^+} - \left.\frac{\partial\psi'}{\partial y}\right|_{y_0^-} = \frac{2\psi'(y_0)\Gamma}{[\bar{u}(y_0) - c]}. \tag{13}$$

Two types of solutions exist for the eigenvalue problem (12): those with symmetric derivatives about y_0 and those with antisymmetric derivatives. If

$$\left.\frac{\partial\psi'}{\partial y}\right|_{y_0^+} = \left.\frac{\partial\psi'}{\partial y}\right|_{y_0^-},$$

then $\psi'(y_0) = 0$ unless $(\bar{u} - c) = 0$ at $y = y_0$. These are the neutral solutions to (12) ($c_i = 0$). They are

[2] Note that these problems arise in a region which does not sustain meridional wave propagation for $c_i = 0$, but where waves are tunneling between propagation regions. See (18) and related text.

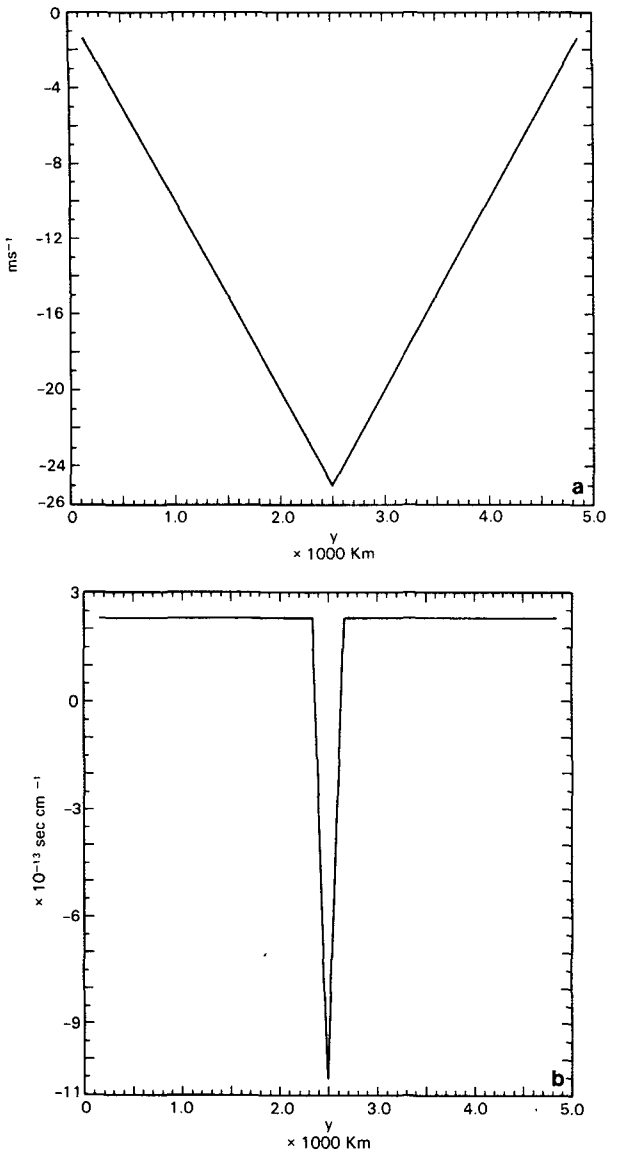

FIG. 1. (a) The mean zonal wind (m s^{-1}); (b) $\partial\bar{q}/\partial y$ for the same profile (s^{-1} cm^{-1}).

neutral because the Rossby waves can not "see" the negative $\partial\bar{q}/\partial y$ region at y_0 since their amplitude is zero there.

When

$$\left.\frac{\partial\psi'}{\partial y}\right|_{y_0^+} = -\left.\frac{\partial\psi'}{\partial y}\right|_{y_0^-},$$

Eq. (12) becomes

$$\left.\frac{\partial\psi'}{\partial y}\right|_{y_0^+} = \frac{\Gamma\psi'(y_0)}{\bar{u}(y_0) - c}, \tag{14}$$

which is the boundary condition used in the Charney problem. The delta function equivalence to the Charney boundary condition was first pointed out by Bretherton (1966). The point jet problem is thus mathematically equivalent to the Charney problem (Lindzen *et al.*, 1983).

As noted by Bretherton (1966) and Taylor (1915), in the presence of rigid boundaries the pv flux integrated over the whole fluid domain must be zero. In addition, away from a CL, the pv flux goes to zero as c_i approaches zero. However, at a CL, there is a jump in momentum flux and from (5a) this implies a downgradient contribution to the pv flux even as $c_i \to 0$ (LT):

$$\int_-^+ (v'q')dy = -\left.\frac{m\pi\beta|\psi'|^2}{2\Gamma}\right|_{y(\mathrm{CL})}. \tag{15}$$

Thus, the pv flux in the neighborhood of the CL is negative. However, in the absence of a sign change in $\bar{q}_y$, there is no possibility of balancing this flux and hence, there can be no solution regardless of c_i. But, when $\bar{q}_y$ does change sign then the negative flux in the neighborhood of the CLs implied by (15) can be balanced by a positive pv flux in the region of negative $\bar{q}_y$, provided $c_i > 0$ (i.e., there must be instability). In the present problem, this positive compensating flux is concentrated at y_0. Using (14) we find

$$F(y_0^+) = -(\overline{u'v'})|_{y_0^+} = \left.\frac{mc_i|\psi'|^2\Gamma}{2|\bar{u} - c|^2}\right|_{y_0^+}. \tag{16}$$

The EP flux for growing (decaying) modes streams outward (inward) from the point y_0. [However, the energy flux for growing (decaying) modes streams inward (outward) from y_0).] Using (4), Eq. (16) implies a positive δ function contribution to the pv flux which is proportional to c_i, i.e.,

$$(\overline{q'v'})|_{y_0} = \frac{\Gamma mc_i|\psi'|^2}{|\bar{u} - c|^2}\,\delta(y - y_0). \tag{17}$$

Now since the negative flux implied by (15) and the positive flux produced at y_0 must balance, Eqs. (15) and (17) could be used to estimate c_i. However, (15) is such a poor approximation to the pv flux at the CL when c_i is finite that using the balance of pv is of little utility.

c. *Numerical solutions of the point jet instability*

Lindzen *et al.* (1983) have analytically computed the dispersion properties of the unstable modes for the eigenvalue problem (12). Here (12) is solved numerically using a 31-point grid over the 5000 km domain. For this grid, $\partial\bar{q}/\partial y$ is shown in Fig. 1b; the dispersion curves are shown in Fig. 2, where the zonal wavenumber is given by $m = N/a$, where a is the earth's radius. We have performed experiments with both 31, 41 and 62 point grids and the results are in good agreement. The low-resolution (31-point) model was used for the widest variety of experiments because of computational cost. We will thus restrict most of our dis-

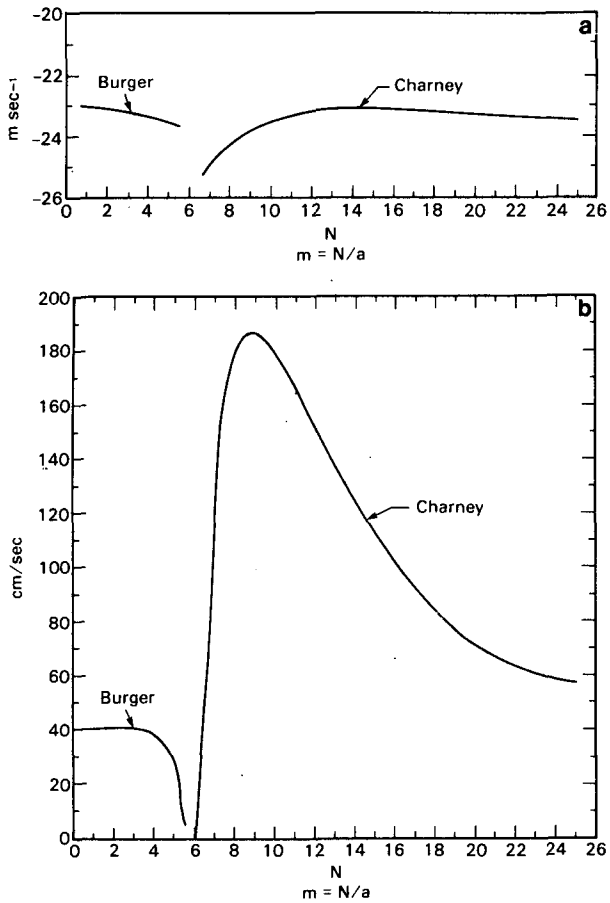

FIG. 2. The (a) real and (b) imaginary phase speeds (c_r and c_i) for barotropic instabilities versus m. Phase speeds are in cm s^{-1}. The growth rate for the unstable mode is $c_i m$.

cussion to results from the low-resolution model, but the results of the 62-point model will be compared for the equilibration experiment.

As is evident in Fig. 2, the fastest growth occurs for $N = 9$. Note also the presence of a neutral point at $N = 6$. Other neutral points occur for smaller values of N but cannot be resolved by the numerical model. The unstable modes for $N < 6$ are often referred to as Burger or Green modes (Burger, 1962; Green, 1960) while modes for $N > 6$ are called Charney modes. For the Charney modes, c_i peaks at $N = 9$ but the slowest eastward moving mode occurs for $N = 14$.

Because of their different character, both the $N = 14$ and $N = 9$ solutions will be examined. In particular, the CLs for the $N = 14$ mode are maximally displaced from y_0 allowing for better numerical resolution of the solution structure. Starting with a Gaussian disturbance, (1) is integrated forward in time. The initial wave amplitude is so small that it produces a negligible effect on the final results. The wave amplitudes obtained after many e-folding growths for $N = 14$ and $N = 9$ are shown in Fig. 3. Since the linear instability can grow to any amplitude, the values shown on the ordinate should be used only for relative comparison. The wave phase (not shown) in both cases increases from the center point out to the boundaries with the most rapid increase taking place in a zone 500 km from the center.

The $N = 14$ mode displays a linearly decreasing amplitude from the center outward to a point roughly corresponding to the end of the $\bar{q}_y < 0$ zone. The wave amplitude then decreases more slowly for a few hundred kilometers and then decreases more rapidly toward the boundary. The $N = 9$ wave also decreases

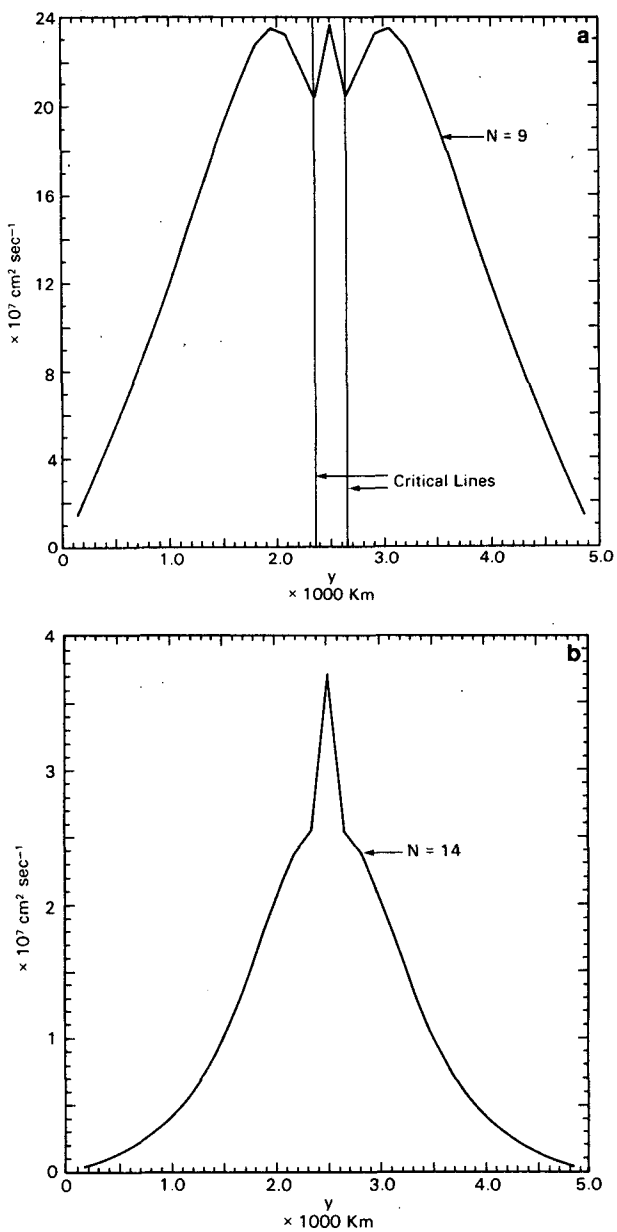

FIG. 3. The amplitude of ψ for (a) $N = 9$ and (b) $N = 14$. Units are cm^2 s^{-1} but scale is arbitrary. Critical lines are noted for the $N = 9$ mode (see also Fig. 4).

linearly out to the $\bar{q}_y = 0$ point, then increases until ~500 km from the center and then rapidly decreases again toward the boundary. The relative phase speed $(\bar{u} - c_r)$ for both modes are shown in Fig. 4. The points where $(\bar{u} - c_r) = 0$ indicate the location of the critical lines or (more accurately) steering levels.

A useful diagnostic is the refractive index function:

$$Q = \bar{q}_y(\bar{u} - c_r)^{-1} - m^2, \tag{18}$$

where $c_r = \mathrm{Re}(c)$. From (12) this function indicates the propagation character of the solution for small c_i. Figs. 5a and 5b show the refractive index function for $N = 9$ and $N = 14$, respectively. The role of m^2 in the refractive index is unimportant except in the boundary regions where $Q \rightarrow -m^2$. The twin maxima in Fig. 5a correspond to the location of the critical lines while in Fig. 5b, the critical lines are located by the sign change in Q marked in the figure. The difference between the two figures results from the relative sign changes in $\bar{q}_y$ and $\bar{u} - c_r$. Since $\bar{u} - c_r$ is negative between the CLs, Q is positive only where $\bar{q}_y$ also becomes negative. In the $N = 9$ numerical calculation, these sign changes occur at the same point (within the resolution of the model) so Q is positive everywhere in the interior zone (locus of y_0). For $N = 14$, Q is positive at y_0 but $\bar{q}_y$ changes sign first (moving from the point y_0 outward) so Q then becomes negative. Further out, $(\bar{u} - c)$ changes sign so Q becomes positive again.

The location of $\bar{q}_y = 0$ and $(\bar{u} - c_r) = 0$ at the same point in Fig. 5a illustrates a basic difference between the numerical and analytical models. In the analytical

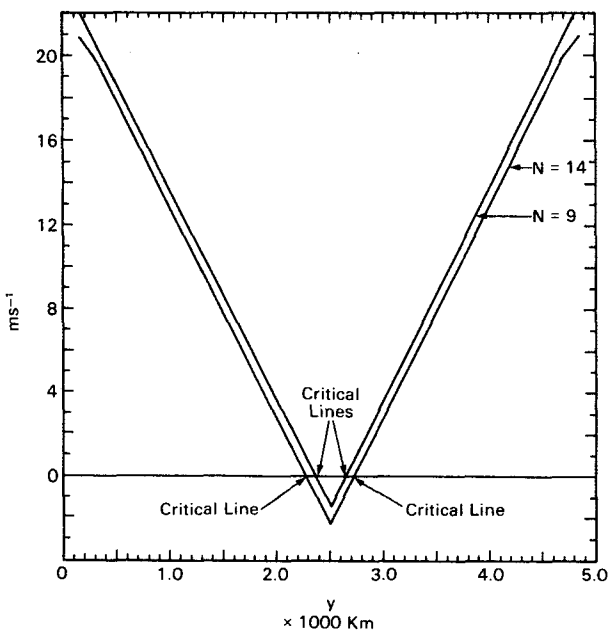

FIG. 4. The relative phase speed $(\bar{u} - c)$ in m s^{-1} for both $N = 9$ and $N = 14$.

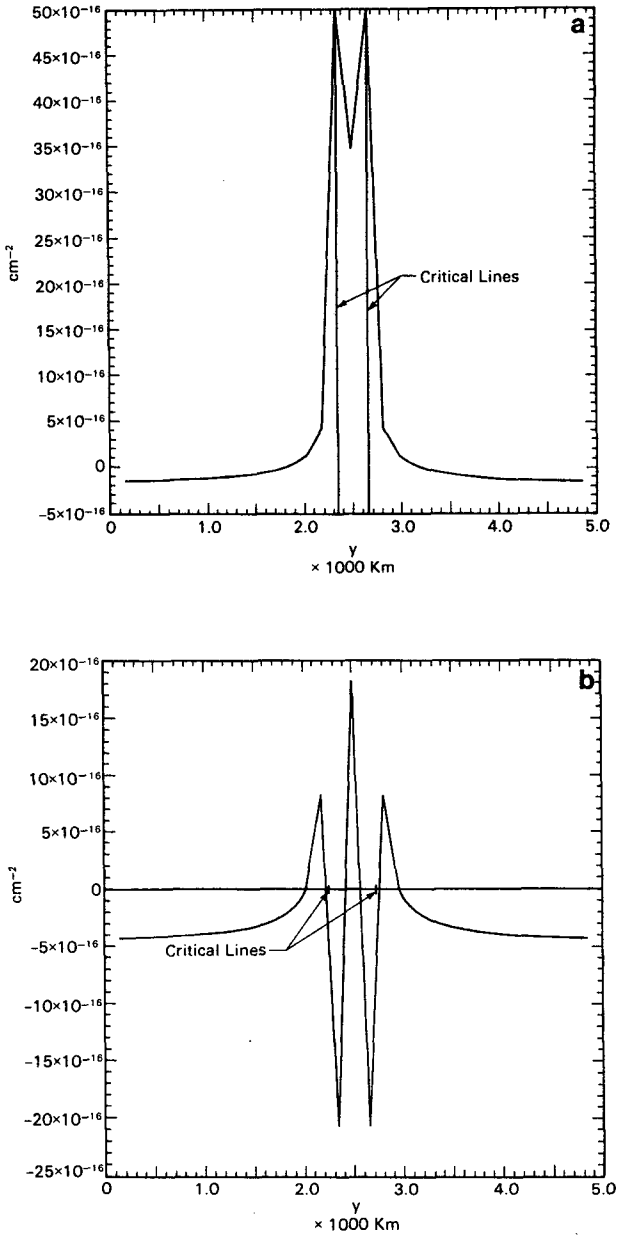

FIG. 5. The propagation function Q for (a) $N = 9$ and (b) $N = 14$. See text for discussion.

model, $\partial\bar{q}/\partial y < 0$ only at y_0 so Q cannot be of one sign unless $c_r = \bar{u}$, which is a neutral solution. Thus, the result shown in Fig. 5a points up the lack of model resolution around the core region (locus of y_0). Nevertheless, the agreement of the model-obtained dispersion curves with the analytical solutions of Lindzen *et al.* (1983) in the Charney domain indicates that the model still accurately reproduces the essential features of the instability. Apparently, the finite difference matching across this layer simulates the detailed structure. A similar behavior is found in the baroclinic two-layer models.

The momentum flux for the two cases is shown in Figs. 6a and 6b. In Fig. 6a, the analytical solution expected as $c_i \rightarrow 0$ is sketched assuming the same location of the critical lines. The convergence of westerly momentum which clearly occurs in the interior zone indicates that the unstable wave decelerates the easterly jet. The difference between the expected analytic solution and the numerical solution is due to the finite value c_i which smears out the momentum flux divergence at the CL. This also explains more rapid decay of the momentum flux toward the outer boundary in Fig. 6b ($N = 14$) which has a smaller c_i compared to Fig. 6a ($N = 9$) for which c_i is larger. Finally, note that the momentum flux is larger for the most unstable mode.

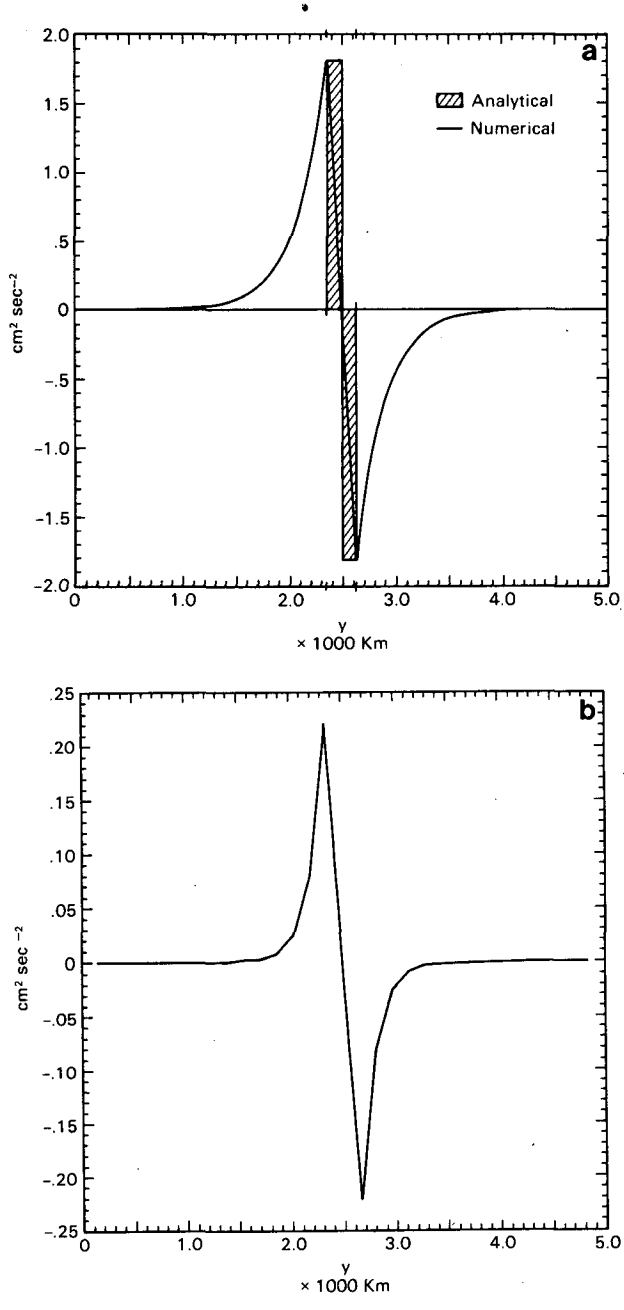

FIG. 6. The momentum flux for (a) $N = 9$ and (b) $N = 14$. The units are cm^2 s^{-2} but scale is arbitrary. Also sketched is the idealized momentum flux for the $c_i \rightarrow 0$ case located at the $N = 9$ critical lines.

From Eq. (15), the momentum flux and energy flux are in the same direction in the inner zone where $(\bar{u} - c_r) < 0$ but have opposite signs where $(\bar{u} - c_r) > 0$. Thus, the energy flux appears to diverge at the CLs and converge at y_0 consistent with the interpretation of wave overreflection.

3. Wave–mean flow interaction

a. Limits on the integrated wave enstrophy

The relation $dq/dt_p = 0$ ($D = 0$) also implies enstrophy conservation,

$$\left.\frac{dq^2}{dt}\right|_p = 0, \tag{19}$$

where p is pressure. Since $q = \bar{q} + q'$, Eq. (19) may be expanded to

$$\frac{d}{dt}(\bar{q}^2 + 2q'\bar{q} + q'^2) = 0.$$

Zonal averaging and integrating from 0 to L gives

$$\frac{\partial}{\partial t}\langle(\bar{q}^2 + \overline{q'^2})\rangle = 0, \tag{20}$$

where $\langle\ \rangle = L^{-1}\int_0^L (\ )dy$. Assuming $\langle\overline{q'^2}\rangle = 0$ at $t = 0$, the above can be integrated to obtain

$$\langle\bar{q}_i^2\rangle - \langle\bar{q}_f^2\rangle = \langle\overline{q_f'^2}\rangle,$$

where the subscript f denotes the final state and i denotes the initial state. Fig. 7 shows $\bar{q}_i$ for the point jet obtained by integrating $\bar{q}_y$ (Fig. 1b) and taking $f_0 = 0$.

Since $\langle\bar{q}\rangle$ is conserved, not all final states for $\bar{q}$ are allowed. For purposes of estimation, we hypothesize that negative zones of $\bar{q}_y$ approach zero in the final state. Two final states which satisfy the criteria that $\langle\bar{q}\rangle$ is constant and $\bar{q}_y \geq 0$ everywhere are shown in Fig. 7. These states are suggested by the wave momentum, pv transport properties, and vorticity mixing, another important idea.

In the unstable basic state, the vorticity gradient is reversed. As the unstable wave develops, the critical lines form and these lines locate the region of the largest particle displacements and the zones of most rapid mixing. Thus, the development of critical lines by the unstable wave suggests a rapid smoothing of the vorticity gradient such as would occur when we move from the initial state to the saturated state (Fig. 7). The idea that intense mixing will occur along the critical line has been discussed previously for stable waves

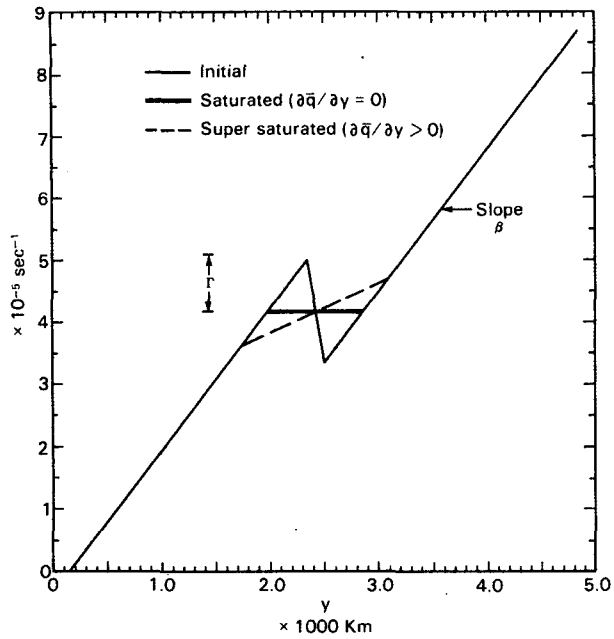

FIG. 7. Sketch of zonal mean vorticity versus y for initial and final states of the instability. See text for discussion.

by Beland (1976), Rhines and Holland (1979) and McIntyre (1980). We expect a similar situation for instabilities.

The initial state has slope β except at y_0; the final state (which we choose) has slope η. The intersection of the slopes for the initial and final states occurs at $y_0 \pm \Gamma(\beta - \eta)^{-1}$ (recall that Γ is the shear). This point should designate the edge of the wave pv transport region, roughly the most distant locus of critical lines. For simplicity we redefine the coordinate system so that y is measured from the center of the point jet at the initial state. Thus,

$$\bar{q}_i = \beta y + \Gamma - 2H(y)\Gamma, \tag{21a}$$

where $H(y)$ is the step function. For the final state,

$$\bar{q}_f = \begin{cases} \beta y + \Gamma, & y < -y_c \\ \eta y, & -y_c < y < y_c \\ \beta y - \Gamma, & y > y_c, \end{cases} \tag{21b}$$

where $y_c = \Gamma/(\beta - \eta)$. Note that the integral $\langle\ \rangle$ need only extend from $\pm y_c$ since $\bar{q}_i = \bar{q}_f$ outside that zone. From (20)

$$\langle \overline{q_f'^2} \rangle = \frac{2\Gamma^3}{3L} \frac{(\beta - 2\eta)}{(\beta - \eta)^2}. \tag{22a}$$

For $\eta = 0$,

$$\langle \overline{q_f'^2} \rangle = 2\Gamma^3/3L\beta, \tag{22b}$$

which is $\sim 6 \times 10^{-12}$ s^{-2} for this problem.

Differentiating (22a) with respect to η gives

$$\frac{\partial}{\partial \eta} \langle \overline{q_f'^2} \rangle = \frac{-4\Gamma^3}{3L} \left[\frac{\eta}{(\beta - \eta)^3} \right]. \tag{23}$$

From (23), $\langle \overline{q_f'^2} \rangle$ maximizes for $\eta = 0$; therefore, (22b) gives the saturation or equilibration limit for which $\bar{q}_f$ is stable for all disturbances while giving the maximum integrated wave enstrophy. For $\eta = 0$, $y_c = \Gamma/\beta$. As η increases above 0, $\langle \overline{q'^2} \rangle$ decreases, moving to zero for $\eta = \beta/2$. Since $\langle \overline{q'^2} \rangle$ cannot be negative, $\eta = \beta/2$ is the oversaturation limit. For the oversaturation limit, $y_c = 2\Gamma/\beta$, twice the equilibration value of y_c.

The physical interpretation of the equilibration and over-equilibration limits are as follows: as the disturbance grows, enstrophy is transferred from the mean flow to the wave. The enstrophy available to the wave is determined by the difference between the mean flow initial and final states. The maximum amount of enstrophy is transferred to the wave when the final state is just stabilized to all disturbances. To overstabilize the final state, vorticity would have to be transferred against a positive gradient of $\partial\bar{q}/\partial y$ so the wave would lose enstrophy in the process.

As noted in Schoeberl (1982), the growth of Rossby waves in a stable basic state produces a final state with regions where $\partial\bar{q}/\partial y$ becomes smaller as the wave transfers pv down gradient. The same process occurs for unstable Rossby waves, but for unstable waves, down gradient transfer tends to stabilize the mean flow ($\partial\bar{q}/\partial y$ increases) liberating enstrophy for the wave. If the same process continues long enough for stable Rossby waves, the flow may become destabilized ($\partial\bar{q}/\partial y$ decreases below zero). The latter process can occur quite readily when Rossby waves propagate vertically. As their amplitude increases in lower density regions of the atmosphere, growing Rossby waves on an isobaric surface can easily produce negative $\partial\bar{q}/\partial y$ regions (Schoeberl, 1983).

The pv distribution in the final state shown in Fig. 7 immediately allows computation of the zonal wind. For an arbitrary final state given by (21)

$$\frac{\partial^2 \bar{u}_f}{\partial y^2} = (\beta - \eta).$$

Thus,

$$\bar{u}_f = \frac{1}{2}(\beta - \eta)y^2 + C_1 y + C_2. \tag{24}$$

The constants C_1 and C_2 are trivially evaluated by noting $\bar{u}_f(\pm y_c) = \bar{u}_i(\pm y_c)$. Thus the parabolic jet is the "simplest" stable configuration. At saturation, $\eta = 0$ so the curvature of the jet is just β.

b. Numerical results without dissipation

The enstrophy limits derived in the previous section are based upon simple stabilization arguments for

wave–mean flow interaction. Yet to be determined is whether the system actually stabilizes in the manner postulated in the previous section. For example, it is conceivable that $\bar{u}$ might vary in such a way as to move the neutral point in Fig. 2b over to the value of N chosen. This, of course, would be unlikely if the initial perturbation consisted of several N's. In addition, even for a single N such an equilibration is unlikely since the neutral point can be only neutral with respect to exponential growth. As shown by Burger (1962), the neutral solution can be associated with fairly rapid linear (not exponential) growth.

To investigate the stabilization process, we integrate the linear instabilities in the previous section foreward in time allowing for wave–mean flow interaction.

1) SINGLE WAVE–MEAN FLOW INTERACTION

In Fig. 8 the integrated enstrophy as a function of time is shown for the two unstable modes $N = 14$ and $N = 9$, as well as the high resolution results for the $N = 9$ case. Also plotted is the value predicted by (22b). The saturation limit predicted in the previous section is in excellent agreement with the numerical results. The two $N = 9$ curves follow each other reasonably well, although not exactly, which suggests that higher resolution may slightly change the details of the results but not their fundamental character. Fig. 9 shows the computed vorticity for $N = 14$ at day 30, shortly after saturation. Clearly, the idealization shown in Fig. 7 is a good approximation of the computed final state. Similar results were obtained for $N = 9$ with both high- and low-resolution models.

Figure 8 also shows that during certain periods the integrated enstrophy slightly exceeds the amount predicted by (22b). This occurs because there is some pv transfer into the central zone ($-y_c < y < y_c$) from outside $-y_c$. For example, slight steepening of the slope of $\bar{q}$ is evident in Fig. 9 near 1500 km. This steepening is due to wave transport of pv near the CLs as they move outward toward the points $\pm \Gamma/\beta$. The net result is that the integrated mean enstrophy of the final state is smaller than that suggested by (22b), so more enstrophy is transferred to the wave. Recall that the minimization referred to earlier assumed that pv transfer takes place only inside the zone $\pm y_c$.

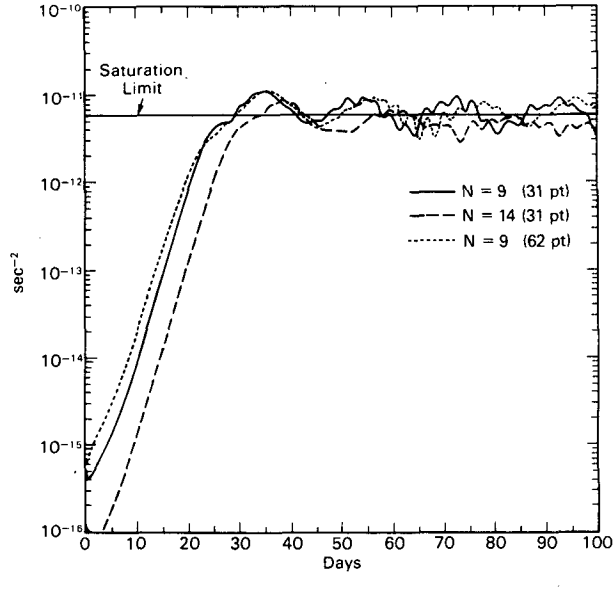

FIG. 8. The channel-integrated enstrophy for $N = 9$ (both 31 and 62 point models) and $N = 14$ versus time. Also marked is the limit suggested by Eq. (22b).

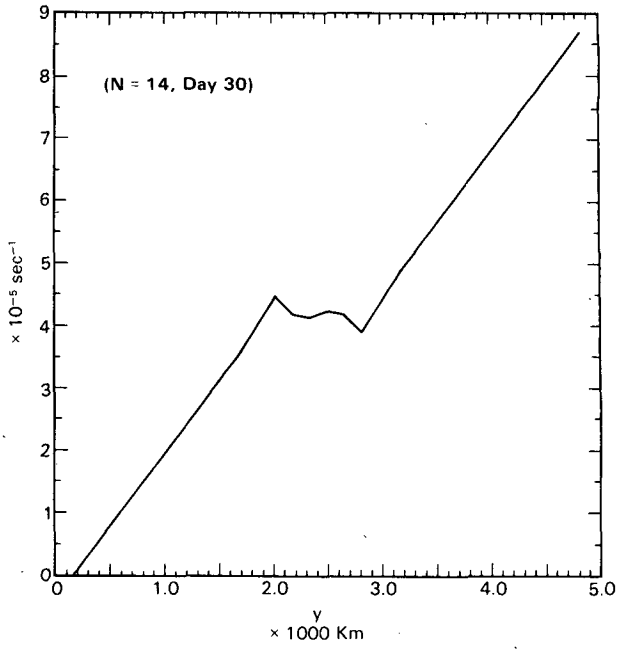

FIG. 9. Zonal mean vorticity for $N = 14$ at day 30.

2) MULTIPLE WAVE–MEAN FLOW INTERACTION

The equilibration limit given by (22b) can be generalized for several waves interacting with the mean flow as well as with each other. In that case, $\langle \overline{q'^2} \rangle$ in (20) becomes a sum of the wave enstrophy for each component, i.e., $\langle \Sigma \overline{q_i'^2} \rangle$.

It is interesting that the fastest growing mode doesn't use up all the available enstrophy before slower growing modes develop large amplitudes. There are several reasons for this. First, the growth rate of the $N = 14$ and $N = 9$ modes are within 14% of each other so they all arrive at "saturation" nearly simultaneously. Second, once the modification of the mean flow has begun, we can no longer identify the fastest growing mode from the linear analysis of the initial state since that state has now been modified. In the modified flow another mode will grow faster than $N = 9$ (assuming that the flow is still unstable) so the other modes can "catch up" and be just as important in the equilibration process as the fastest growing mode in the linear regime.

Figure 10 shows the integrated enstrophy when waves $N = 9$, 12 and 14 interact with the mean flow but not with each other through wave–wave interaction. Also marked ($S/3$) is the line having a slope one-third that of Eq. (22b). Although each wave has a different growth rate, at saturation the average enstrophy (over a long period) is nearly equally partioned between them since they tend to follow the $S/3$ line. Statistically, the saturation limit for multiple waves is simply given by

$$\overline{\langle q_j'^2 \rangle} = \frac{2\Gamma^3}{3L\beta^2 k},$$

where j is the jth zonal wavenumber and k is the total number of waves. Nevertheless, the interaction of the waves through the mean flow can produce periods where the enstrophy of a single component is much larger than the remaining components. This whole process is analogous to the statistical mechanics description of the equilibrium distribution of particles with a single degree of freedom. The results obtained in this case are independent of the initial (very small) wave amplitudes.

c. *Numerical results with dissipation*

In the presence of dissipation, equipartition of wave enstrophy would not be expected after long times since the equilibration processes are different. Using the same procedure as in Section 3a, however, a distinct limit may be developed for the behavior of unstable waves in the presence of dissipation. First, note that the role of dissipation in the mean flow equation is different from that in the wave equation. In Eq. (1) wave pv is always lost by dissipation but in Eq. (2), mean flow pv can be both generated or lost depending on whether $\bar{q} < q_0$ or $\bar{q} > q_0$. If a steady state solution to the system of equations is produced then the pv generation in regions where $\bar{q} < q_0$ must balance the mean flow pv loss where $\bar{q} > q_0$ and wave loss of pv. The transport of pv from the source to the sink regions is accomplished by the dissipating wave. [The nonacceleration or nontransport theorem requires that pv transport be zero at steady state *unless* dissipation is present (Andrews and McIntyre, 1978).]

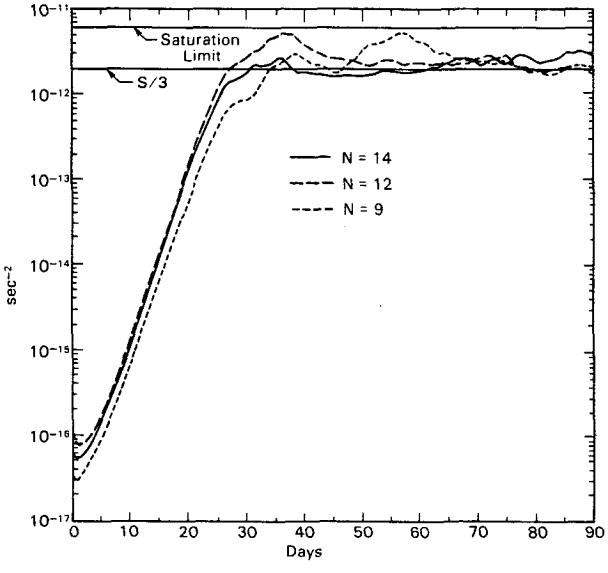

FIG. 10. The integrated enstrophy for a multiple wave instability. Limits from Eq. (22b) and that assuming equipartition of enstrophy are also shown.

For the simple form of dissipation used in (1) and (2) the steady state enstrophy equation can be derived:

$$\langle \bar{q}^2 \rangle - \langle q_0 \bar{q} \rangle = -\overline{\langle q'^2 \rangle}, \tag{25}$$

where the time scale relevant to equilibration is D^{-1}. Assuming the equilibrium initial state $q_0 = \bar{q}_i$ defined in (21a) and $\bar{q} = \bar{q}_f$ defined in (21b) we obtain

$$\overline{\langle q'^2 \rangle} = -\frac{\Gamma^3 \eta}{3L(\beta - \eta)^2}. \tag{26}$$

Since $\langle \bar{q}'^2 \rangle$ is positive definite, η must be negative. Thus, the criterion (25) is not a stable configuration (i.e., $\bar{q}_y < 0$) and any instability whose growth rate (mc_i) exceeds D can continue to develop. In general, it is straightforward to show that all solutions to (26) are unstable. Note that the dissipation parameter D disappears from (25) indicating a balance between the forcing of the wave–mean flow system and damping.

Even though we can compute the wave enstrophy given a model like (21a), there is no *a priori* reason to suspect that the function (21a) bears any resemblance to an actual final state. In order to determine the final state, we have run several experiments where large amounts of dissipation were applied after the wave had reached the saturation amplitude. The results are shown in Fig. 11a. In both experiments shown, and all cases we have examined, the integrated wave enstrophy asymptotes to the same value for a given wavenumber. The only apparent role the magnitude of the dissipation has is to hasten the approach to the asymptotic limit. For other wavenumbers the asymptotic value is usually smaller; for example, for $N = 14$ the asymptotic value for the integrated wave enstrophy is 1.16×10^{-12} s^{-1}, while for $N = 9$ the asymptotic value is 1.36×10^{-12} s^{-1}. Note that if the very strong dissipation were applied in the linear growth phase and $D \geqslant mc_i$, the wave would dissipate.

The results shown in Fig. 11a and Eq. (26) suggest that waves, once established, may be present in an unstable environment even though the dissipation is large. The origin of the waves is a secondary question; they may have propagated from other regions or be forced by other processes.

In Fig. 11b the zonal mean vorticity at day 200 (the final state) is shown. Also shown are two analytic models representing the vorticity distribution in the core region. These models are simplified constructs of the

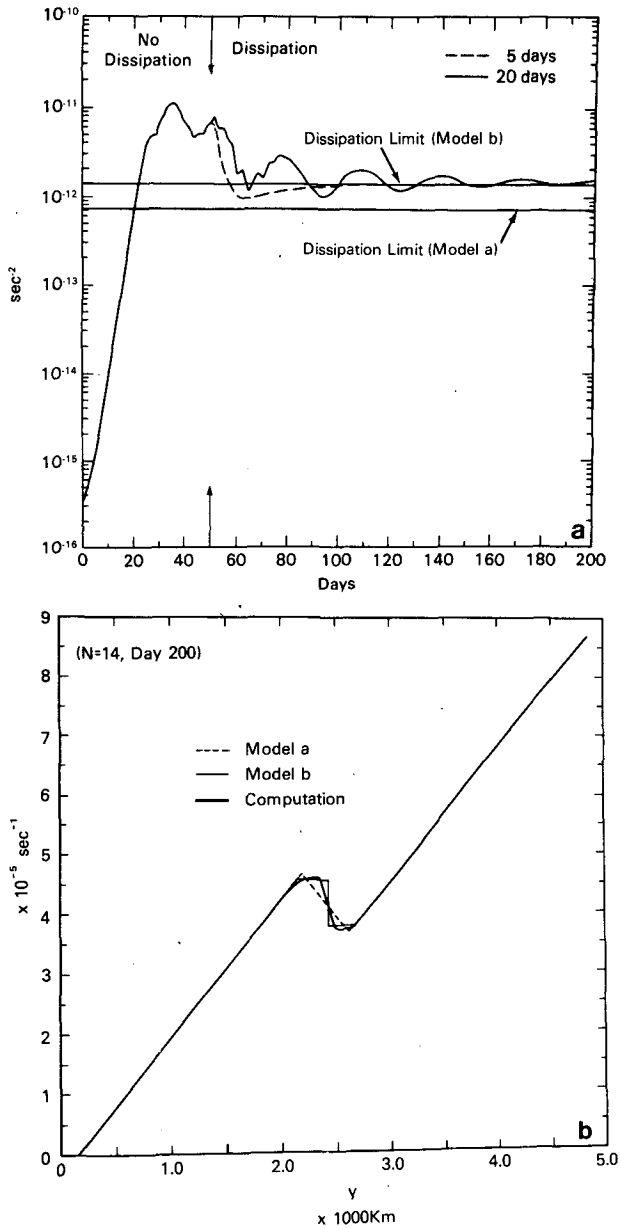

FIG. 11. Dissipation experiments for the $N = 9$ mode. (a) The integrated wave enstrophy versus times (as in Fig. 8) until day 50 where strong dissipation is applied. The time scale for the dissipation D^{-1} in days, is given in the figure. (b) The mean vorticity ($\bar{q}$) at day 200 and the analytic Models a and b (see Section 3c).

numerically generated final state and other constructs could also be considered. The first model (Model a) is obtained by differentiating the function (26) to obtain the maximum value. For Model a, Eq. (26) maximizes for $\eta = -\beta$, $y_c = \Gamma/2\beta$. For which

$$\langle \overline{q'^2} \rangle = \frac{1}{8}(22b) \approx 7.5 \times 10^{-13}\ \mathrm{s}^{-1}, \qquad (27)$$

which is about half the asymptotic value shown in Fig. 11a. Another model which better reproduces the "flat top" features apparent in Fig. 11b (which also appears in the higher resolution simulations) is given by

$$\bar{q} = \begin{cases} \Gamma - \beta r, & -r < y < 0 \\ \beta r - \Gamma, & 0 < y < r. \end{cases} \qquad (28)$$

Using this function yields,

$$\langle \overline{q'^2} \rangle = \beta r^2(\Gamma - \beta r)/L. \qquad (29)$$

Then for Model b, the maximum of (29) occurs for $r = 2\Gamma/3\beta$ or for

$$\langle q'^2 \rangle = \frac{2}{9}\,\mathrm{Eq.}\ (22b) \approx 1.3 \times 10^{-12}. \qquad (30)$$

While this model predicts a result closer to the computed value, it probably overemphasizes the magnitude of $\partial\bar{q}/\partial y$ at the core. Neither Model a nor Model b are ideal choices for the final state, but Model b appears to give a better representation as far as the integrated enstrophy. It is interesting to note that the wave–mean flow system always seeks to maximize the wave enstrophy even when no growth occurs.

Figure 12 shows the change in the integrated enstrophy with dissipation present for the same multiple wave case shown in Fig. 10. Only the fastest growing mode ($N = 9$) survives after long times and the solution appears to asymptote to the limit given by (30). Finally, it is quite apparent that the equipartition of enstrophy does not occur in the present of dissipation.

4. Discussion

Determining constraints on barotropic instabilities which have evolved past the linear phase (where wave–mean flow and wave–wave interaction may be neglected) is important for geophysically realistic flows. As the unstable Rossby wave modifies the zonal flow, its structure changes. (One way of viewing this process is that once the mean flow starts to change, the basic

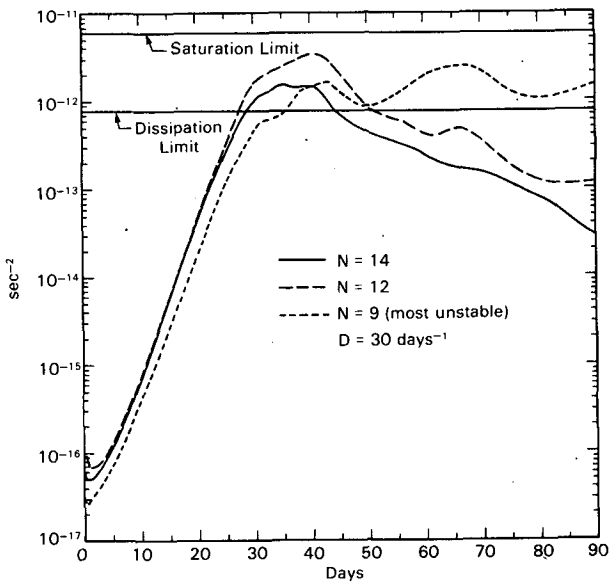

FIG. 12. As in Fig. 10 but with dissipation. Also shown are limits from Eq. (22b) (upper limit) and Eq. (30) (asymptotic limit). The damping time scale is 30 days.

state is now most unstable to a mode with a slightly different structure). In the case of the point jet instability, the wave transports westerly momentum into the jet and smooths out the point to a parabolic curve.

In order to produce a smooth jet profile the critical lines move outward to the approximate positions $\pm \Gamma/\beta$ from the core *independent* of their initial position. To position the critical lines at $\pm\Gamma/\beta$ the phase speed of the mature instability must therefore decrease to $\bar{u}(y_0) + \Gamma^2/\beta$, at $y_0 \pm \Gamma/\beta$, where $\bar{u}(y_0) = -25$ m s^{-1} in this problem. This idealized picture has been verified by the numerical model. However, after the critical lines reach $\pm\Gamma/\beta$, the structure of the mature instability becomes quite complicated with multiple meridional modes as well as free modes appearing when the growth rate slows. Detailed analysis of the statistically equilibrated instability will be deferred to future work.

Even though the behavior of the equilibrated instability is complex, the enstrophy limits derived in Section 3 appear to provide accurate information after long times on the behavior of the system. The limit (22a,b) provides a practical upper bound for the maximum integrated wave enstrophy. The dissipation limit suggested by Model b [Eq. (28)–(30)] gives a good approximation to the asymptotic value of the integrated wave enstrophy when it has equilibrated with the mean flow. The asymptotic state is 1) independent of the magnitude of the dissipation and 2) always unstable by the Rayleigh-Kuo criteria. Unfortunately since the structure of the saturated wave disturbance may be considerably different from the linear structure, the integrated enstrophy is not very useful for estimating the wave amplitude in either of the saturation or dissipation limits.

The role of wave–wave interaction has not been explored in this work; however, we have obtained preliminary results from a high-resolution, fully nonlinear model of the point jet instability. We have found that the processes of instability equilibration in the fully nonlinear is almost identical with the wave–mean flow interaction model which suggests that our main conclusions are not significantly altered by the lack of wave–wave interaction. The results of the fully nonlinear studies will be presented in Part 2.

Finally, we note that even though the point jet instability is mathematically similar to the Charney problem for baroclinic instability, the stabilization mechanism for baroclinic instability is, at least superficially, more complicated. Even if equilibration in baroclinic instability only involved the elimination of region's of negative $\bar{q}_y$ it is not clear what combination of changes in $\bar{u}(y, z)$ and the static stability would lead to such a state.

Acknowledgments. We would like to acknowledge computational support from the Space Plasma Computer Analysis Network (SCAN) as well as helpful comments from Conway Leovy and the reviewers. R.S.L. was supported by NSF Grant ATM-82-05638 and NASA Grant NGL 22-007-228.

REFERENCES

Andrews, D., and M. McIntyre, 1976: Planetary waves in horizontal and vertical shear. The generalized Eliassen-Palm relation and the mean zonal acceleration. *J. Atmos. Sci.*, **33**, 2031–2048.

—— and ——, 1978: Generalized Eliassen-Palm and Charney-Drazin theorems for waves on axisymmetric mean flows in compressible atmospheres. *J. Atmos. Sci.*, **35**, 175–185.

Beland, M., 1976: Numerical study of the nonlinear Rossby wave critical level development in a barotropic zonal flow. *J. Atmos. Sci.*, **33**, 2065–2078.

Bretherton, F. P., 1966: Critical layer instability in baroclinic flows. *Quart. J. Roy. Meteor. Soc.*, **92**, 325–334.

Burger, A. P., 1962: On the non-existence of critical wavelengths in a continuous baroclinic stability problem. *J. Atmos. Sci.*, **19**, 31–38.

Charney, J. G., 1947: The dynamics of long waves in a baroclinic westerly current. *J. Meteor.*, **4**, 135–162.

——, 1973: Planetary fluid dynamics. *Dynamic Meteorology*, P. Morel, Ed., D. Reidel, 97–351.

——, and P. G. Drazin, 1961: Propagation of planetary-scale disturbances from the lower into the upper atmosphere. *J. Geophys. Res.*, **68**, 6441–6442.

——, and M. E. Stern, 1962: On the stability of internal baroclinic jets in a rotating atmosphere. *J. Atmos. Sci.*, **19**, 159–172.

Dickinson, R. E., 1968: Planetary Rossby waves propagating vertically through weak westerly wind wave guides. *J. Atmos. Sci.*, **25**, 984–1002.

Edmon, H. J., B. J. Hoskins and M. E. McIntyre, 1980: Eliassen-Palm cross sections for the troposphere. *J. Atmos. Sci.*, **37**, 2600–2616.

Green, J. S. A., 1960: A problem in baroclinic stability. *Quart. J. Roy. Meteor. Soc.*, **86**, 237–251.

Lindzen, R. S., and K. K. Tung, 1978: Wave over-reflection and shear instability. *J. Atmos. Sci.*, **35**, 1626–1632.

——, and M. R. Schoeberl, 1982: A note on the limits of Rossby wave amplitudes. *J. Atmos. Sci.*, **39**, 1171–1174.

——, B. Farrell and K. K. Tung, 1980: The concept of wave overreflection and its application to baroclinic instability. *J. Atmos. Sci.*, **37**, 44–63.

——, A. J. Rosenthal and B. Farrell, 1983: Charney's problem for baroclinic instability applied to barotropic instability. *J. Atmos. Sci.*, **40**, 1029–1034.

McIntyre, M. E., 1981: How well do we understand the dynamics of stratospheric warmings? *J. Meteor. Soc. Japan*, **60**, 37–65.

Palmer, T. N., 1982: Properties of the Eliassen-Palm flux for planetary scale motions. *J. Atmos. Sci.*, **39**, 992–997.

Rhines, P. B., and W. R. Holland, 1979: A theoretical discussion of eddy driven mean flows. *Dyn. Atmos. Oceans*, **3**, 289–325.

Schoeberl, M. R., 1981: A simple model of the Lagrangian-mean flow produced by dissipating planetary waves. *J. Atmos. Sci.*, **38**, 1841–1855.

——, 1982: Vacillation, sudden warmings and potential enstrophy balance in the stratosphere. *J. Atmos. Sci.*, **39**, 1862–1872.

——, 1983: A study of stratospheric vacillations and sudden warmings of a β-plane. Part I: Single wave–mean flow interaction. *J. Atmos. Sci.*, **40**, 769–787.

Simmons, A. J., and B. J. Hoskins, 1978: The life cycles of some nonlinear baroclinic waves. *J. Atmos. Sci.*, **35**, 414–431.

Simons, T. J., 1972: The nonlinear dynamics of cyclone waves. *J. Atmos. Sci.*, **29**, 38–52.

Taylor, G. I., 1915: Eddy motion in the atmosphere. *Phil. Trans. Roy. Soc. London*, **A215**, 1–26.

Tung, K. K., 1981: Barotropic instability of zonal flows. *J. Atmos. Sci.*, **38**, 308–321.